Simulation of high-specific-impulse and double-stage Hall thrusters

IEPC-2005-040

D. Escobar,[*] A. Antón,[†] and E. Ahedo[‡]

Universidad Politécnica de Madrid, Spain

A two-dimensional, hybrid code for simulation of dual-mode Hall thrusters is being developed. Results are presented for the evolution of thruster performances with the discharge voltage. Particular attention is paid to the effect of doubly-charged ions. The code is accepting the presence of intermediate electrodes at the chamber walls. A sheath model for these electrodes is being developed. First results for two-stage discharges are presented.

I. Introduction

Recent trends in Hall thruster design have shown an increasing interest on dual-mode efficient operation. The advantages are clear for this type of operation: on the one hand, a high thrust but low specific impulse regime allows for efficient orbit raising where the minimization of the transfer duration is the main constraint; on the the other hand, orbit correction missions such as north-south station keeping can take advantage of the high specific impulse regime, which minimizes the mass consumption.[1]

Several programs have already been launched in the last few years to design and qualify dual-mode Hall thrusters and the main problem that still remains is the operation at high specific impulse (or high discharge voltage). It is usually found experimentally that a decrease on efficiency appears at voltages higher than 600V-700V and it is claimed that one of the possible reasons for this to happen is, among others, the generation of doubly-charged ions, leading to ion populations of very different average velocities at the thruster exhaust.

However, recent results from Hofer and Gallimore[2] have shown that a monotonically increasing efficiency is possible if the magnetic field topology is optimized for high discharge voltages. Thus, disadvantages of multiple ionization seem not to be the only reason for the efficiency decrease at high specific impulse operation measured in other experiments.

A promising Hall technology for dual-mode operation is the two-stage design where an intermediate electrode is used to enhance the ionization and acceleration processes. Although the theoretical advantages of this type of thrusters are obvious, experiments tend to show that no clear benefit appears when two-stage operation is used.[3–5] This might be due to a poor understanding of the physical processes involved in this kind of thrusters where the intermediate electrode can change significantly the discharge characteristics. Recently, Ahedo and Parra[6] published a model of the two-stage discharge where they demonstrate that performance and efficiency depend much on the position and current of the intermediate electrode and,

---

[*]Student, Escuela Técnica Superior de Ingenieros Aeronáuticos(ETSIA), escobar@fmetsia.upm.es.
[†]Student, ETSIA, alfredoanton@fmetsia.upm.es.
[‡]Associate Professor, ETSIA, eduardo.ahedo@upm.es.

technical issues apart, predict relative efficiency enhancements of 20% for optimal values of the intermediate electrode parameters.

This paper presents numerical results of Hall thrusters operating at high-specific impulse with single- and double-stage designs. The goal of these simulations is two-fold. On the one hand, we aim to better understand the plasma discharge at these operation conditions. On the other hand, we use them for testing a new simulation code based on HPHall-2,[7] an upgraded version of Fife's HPHall.[8] The paper is organized as follows. Section II comments the innovative points we are trying to implement on the new simulation code. Section III presents results for high-specific impulse and single-stage operation. Section IV shows preliminary results for a two-stage discharge. Section V is devoted to erosion of the wall chambers and its effect on performances.

II.   On the simulation code

HPHall-2[7] is a two-dimensional(2D), hybrid, and quasineutral code. Heavy species are modelled with a particle-in-cell plus Monte-Carlo Collision(PIC-MCC) method while electron are modelled macroscopically. This procedure is a good trade-off between fully fluid models, which are not well suited for Hall thrusters where particle densities are too low, and fully kinetic models where computational time is enormous. In addition, HPHall-2 assumes cylindrical symmetry, lateral ceramic walls, and uses an externally-imposed magnetic field, B. Figure 1 shows the different elements of the simulated thruster, the mesh used by the PIC part of the code, the magnetic field profile at the channel median, and the magnetic streamsurfaces used by the electron subcode. Macroscopic magnitudes for ions and neutrals (density, flux, temperature,...) are computed by weighting particle magnitudes at every node of the mesh. Typical numbers of macro-particles are 30.000 per species (ions and neutrals) and about 1000 cells in the mesh.

The strong magnetic field causes a high anisotropy in the electron macroscopic dynamics, which allows to treat in different manner the directions parallel and perpendicular to B. In particular, Boltzmann equilibrium is assumed along magnetic lines while an Ohm's law (with pressure effects) is used in the perpendicular direction. In HPHall-2 the 2D energy equation is transformed into a 1D problem by first integrating electron equations in volumes bounded by the walls and two magnetic field lines. The main outputs of the electron sub-code are the electron temperature, necessary to evaluate collisional processes, and the electric potential, which defines the electric field to be applied on ions. Finally, since the code is quasineutral, the simulation boundaries are not the walls but the transition surfaces to the space-charge sheaths tied to the chamber walls. This requires to solve independently the different sheath problems in order to define the correct conditions at the boundaries of the quasineutral domain.
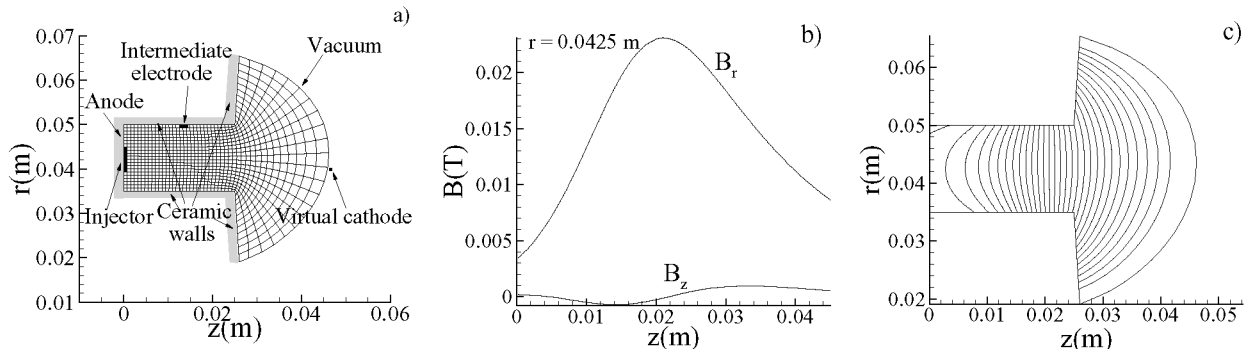
Figure 1.   Elements of the simulated SPT-100 type simulated thruster and PIC-mesh(a), reference magnetic field at the chamber median, B_r and B_z are the radial and axial components respectively(b) and magnetic streamsurfaces used in the electron-mesh(c).

Based on HPHall-2 fundamentals, we decided to work on a new simulation code with two categories of objectives:

1. A better modelization and more accurate algorithms of the main phenomena of the discharge. This

includes:

(a) Implementation of more accurate sheath models.

(b) Improvement of magnitude weighting at the boundaries. These two issues are treated in a parallel paper.[9]

(c) Detailed treatment of the near anode region for oblique magnetic fields. The difficulty lies in matching the 1D electron equations at each magnetic line to the anode sheath boundary, which is not a streamline. The handling of boundary conditions for the case of an anode sheath, that can be electron-repelling in certain zones and ion-repelling in others, is an important issue, partially unsolved yet.

(d) The development of a more accurate electron subcode. A new differential formulation of the electron equations, totally based on curvilinear magnetic coordinates is being derived. Modified algorithms try to increase the spatial and temporal accuracy of the solution. Effects previously neglected like electric work parallel to B-lines is being included. A modification of the constant-temperature, Boltzmann equilibrium model in the B-parallel direction is pending on advances on a parallel research on the electron distribution function.[10] A more detailed model of anomalous diffusion is pending too on advances on a parallel research.[11]

(e) Improvement of algorithms for moving and injecting particles in the PIC subcode. The objective is a reduction of temporal errors by one-order of magnitude. Apart from obtaining a higher accuracy, this will allow to carry out long runs and numerically-reliable parametric studies.

2. To increase the capabilities of the code.

(a) High specific impulse performances. Double ions become a significant population at high discharge voltages. The new code includes (~ 30.000)double ions at a separate species. Effects of double ions on the sheath conditions are included too. A higher flexibility on the magnetic meshes that the electron subcode can manage easily is necessary.

(b) Two-stage discharges. This consists mainly on considering the presence of internal electrodes in certain regions of the inner or outer walls. For the code, it implies, at least: (1) another major modification on the electron subcode, since the discharge current cannot be considered constant along all magnetic streamlines; (2) the formulation of a sheath model for different electrode types, in particular for highly-emissive ones; (3) modifications of the PIC subcode in those regions where the space-charge sheaths become ion-repelling; and (4) to take into account the external electric circuit on the wall and sheath boundary conditions.

(c) Implementation of algorithms to compute erosion of the chamber walls and its effects on the thruster performances.

The Hall thruster taken as reference for the computations here is of the SPT-100 type, which is characterized by the following nominal properties:

V_d	$\dot{m}$	B_{max}		P_d	η	F	I_{sp}
300 V	4.8 mg/s	230 G		1350 W	0.48	83 mN	1600 s

Table 1. SPT-100 nominal operating and performance parameters.

The simulation results obtained with the conditions sketched in Fig.1 for the above operating parameters are

Clearly, this simulation underestimates thruster efficiency. There are two kind of reasons. First, no attempt was made to optimize the 'empirical' parameters of the model, like the anomalous diffusion or the wall accommodation coefficients, both having a relevant impact on performances. The second reason lies on the plasma-wall interaction model, which leads to excessively high plasma recombination and energy losses at the walls. Depletion of the the tail of primary electrons,[12,13] two electron temperature models,[14] and partial

P_d	η_a	F	I_{sp}
1007 W	0.38	61 mN	1289 s

Table 2. SPT-100 simulated performance parameters.

trapping of secondary emission[15] have been suggested to modify the common plasma-wall interaction model. In an effort to treat these phenomena in a single and consistent frame, Ref. 10 presents first results on a kinetic model of the electron distribution function with partial thermalization. This model should ultimately give the clues to improve the electron macroscopic model used by the code. Apart from this overestimate of wall losses, the code is capable of reproducing well the main physical aspects of the discharge and can be used to analyze (qualitatively, at least) the influence of different operating parameters as discharge voltage or mass consumption.

III.   High-specific impulse operation

A.   Influence of doubly-charged ions

As the discharge voltage increases, the electron temperature increases thus augmenting the multiple ionization fraction. The novelty in this code is to treat doubly-charged ions as an independent species from singly-charged ions. This allows to have reliable weighting magnitudes for these particles. The penalty is an increase of a 20% in computational time although, for a typical case, the total time remains within the order of an hour for a 2.4GHz PC.

A non-dimensional parameter that measures the relative importance of doubly-charged ions is the local ion charge number

$$Z_i \equiv \frac{n_e}{n_i} = \frac{n_{i+} + 2n_{i++}}{n_{i+} + n_{i++}}, \tag{1}$$

which usually takes values between 1 and 1.1. Definitions of thruster efficiencies in the presence of double ions are given in the Appendix. Figure 2 shows, for the nominal case of Sec. II, the effect of including double ionization. Even for this moderate voltage, 300V, the anode efficiency η_a increases a 5%, from 0.378 to 0.397, mainly due to a higher propellant utilization. Notice how the charge number increases with the temperature from the anode until the maximum T_e. Downstream of this point, the charge number value is due to ion convection. The charge utilization is η_q =0.993. Hofer and Gallimore obtained experimentally, for the NASA-173Mv2 thruster and 300V, a lower value, η_q =0.986, which means larger multiple ionization even.
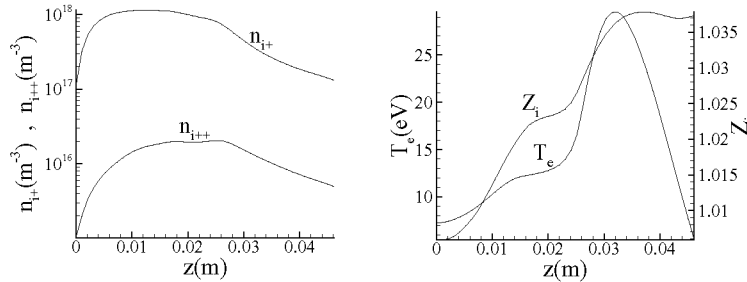
Figure 2. Singly- and doubly-charged ion densities along the channel, n_{i+} and n_{i++} respectively,(left figure) and electron temperature T_e and equivalent ion charge number Z_i along the channel (right figure). All variables are evaluated at the chamber median, r= 0.0425m.

B. Influence of the discharge voltage

Figure 3 displays the variation of the main parameters when the voltage is increased from 300V to 750V, and the magnetic field strength is increased proportionally to V_d; the rest of parameters remain nominal. As expected, the specific impulse and the thrust increase proportionally to $V_d^{1/2}$ rather well. Deviations are due to variations on propellant and voltage utilizations. The total discharge current remains constant through the entire range of variation of V_d due to the variation of the magnetic field strength commented above. As a consequence, the total power varies proportionally to the discharge voltage.

Efficiency increases up to 600V where a peak is found. The posterior decrease seems to be caused both by higher wall losses and a decrease of voltage utilization and plume divergence efficiency. The same parametric investigation has been performed switching off multiple ionization and the peak of efficiency remains. This contradicts the common argument that the decrease of efficiency at high voltages is due to doubly-charged ions, but seems to agree with Hofer and Gallimore who obtained a monotonically increasing efficiency by optimizing the magnetic field topology.
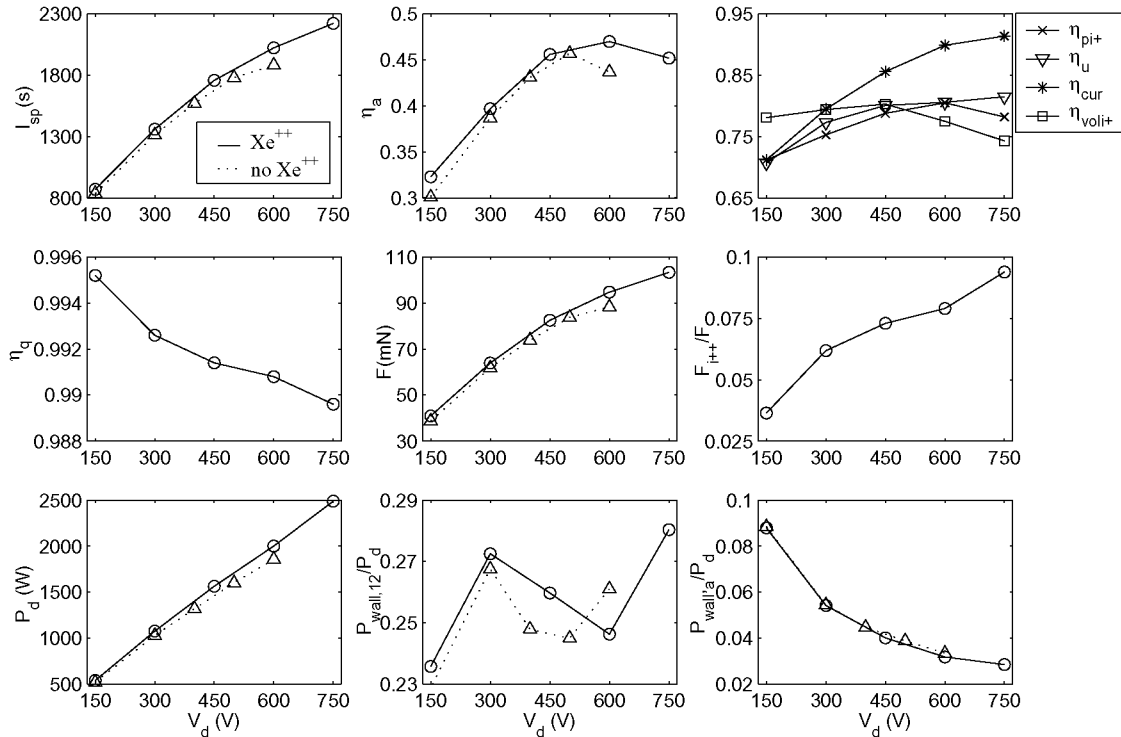
Figure 3. Variation of main operation parameters when varying the discharge potential V_d. $P_{wall,12}$ and $P_{wall,a}$ represent total energy losses to inner and outer walls and to the anode.

Multiple ionization influence is quantified by the charge utilization efficiency, η_q, and the contribution to thrust of doubly-charged ions (F_{i++}/F). At 750V the contribution of doubly-charged ions to thrust is as high as 10%, which emphasizes the importance of including and modelling them properly.

Figure 4 shows 2D plots of the discharge at three discharge voltages. Figures 5 and 6 display profiles at the channel median and outer wall, respectively. In all cases, time-averaged magnitudes (excluding initial transients) are plotted. Relative energy losses at the walls tend to decrease when increasing V_d except for the limiting case of 750V. This reduction on wall losses is due to a better acceleration process which prevents the ions from reaching the walls as shows the profile of the ion current to the outer wall, j_{Wi}, in figure 6. The anomaly encountered at 750V seems to be caused by a temperature peak inside the ionization chamber as it is shown on figure 5. This peak causes higher wall losses and modifies the electric potential fall through the channel. The optimized magnetic field topology proposed by Hofer-Gallimore in order to increase efficiency at high voltages is characterized by a near zero magnetic field strength precisely where our model predicts a

The 29th International Electric Propulsion Conference, Princeton University,
October 31 - November 4, 2005
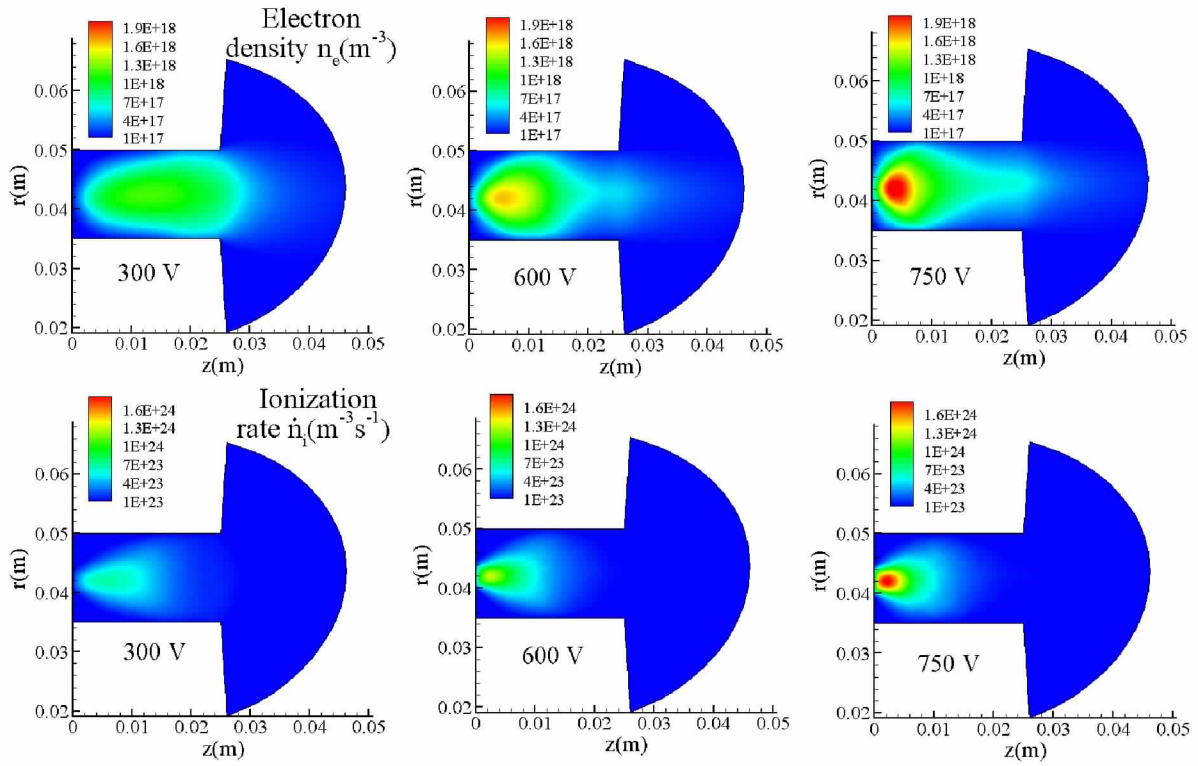
Figure 4. Electron density, n_e (upper figures), and total ionization rate, $\dot{n}_i$ (lower figures) at $V_d = 300$ V, 600 V and 750 V, for the previous parametric variation.
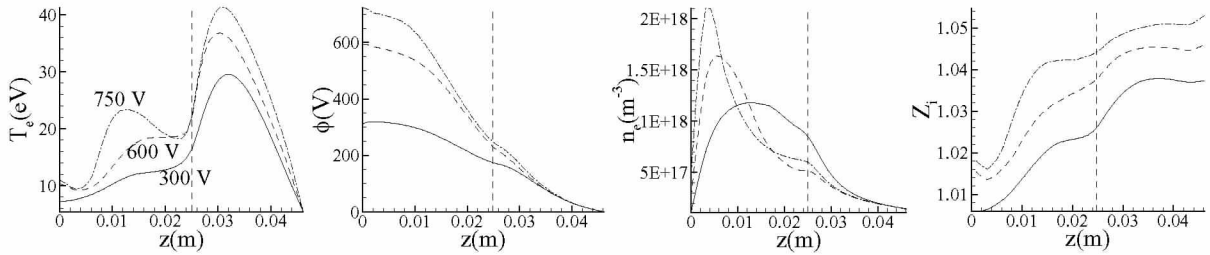
Figure 5. Electron temperature T_e, electric potential ϕ, electron density n_e and equivalent charge number Z_i profiles at different discharge voltages ($V_d=$ 300 V(solid), 600 V(dashed) and 750 V(dashed-dotted)). All variables are evaluated at the chamber median (r=0.0425m). The vertical dashed line represents the thruster exit.
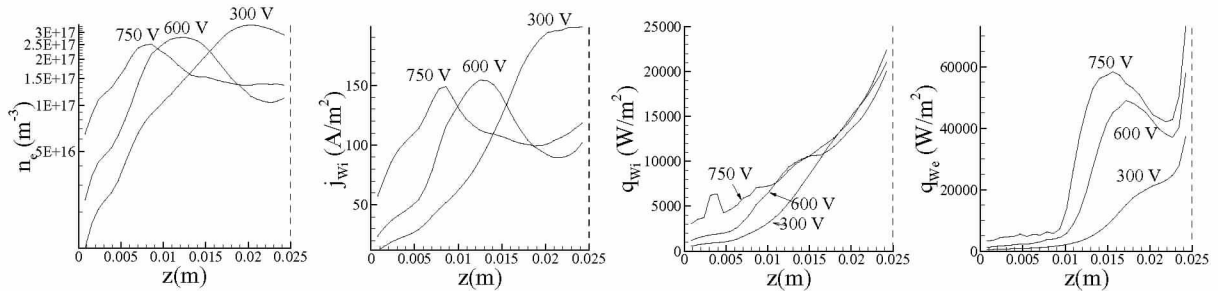
Figure 6. Electron density, n_e, ion current to wall, j_{Wi}, ion energy flux to wall, q_{Wi}, and electron energy flux to wall, q_{We} for $V_d=$ 300 V, 600 V and 750 V. All variables are evaluated at the outer wall (r=0.05m). The vertical dashed line represents the thruster exit.

peak on temperature. Thus, it must be numerically checked whether a magnetic field topology like that one could avoid the peak temperature and improve efficiency at high voltages.

Figure 5 also plots the plasma density and equivalent charge number. Due to electron pressure and electric acceleration, the plasma tends to be confined near the anode for higher voltages. Thus, the ionization process is confined to that region too, as shown in figure 4.

IV.   Two-stage discharges

A.   Sheath model for active electrodes

Active electrodes are the preferred method when designing two-stage SPT-type Hall thrusters. Generally this intermediate electrode is made of a high electron emissivity material.

This new element inside the chamber requires proper modelling and in particular, the plasma-wall interaction problem is modified with respect to the ceramic wall case treated in 16 and 9. The model we are implementing considers an active electrode operating continuously in the charge saturated regime(CSR) due to its high electron emissivity. The potential of the electrode should be a known parameter, whereas the electric current through the electrode would be the output. However, at present, and because of the unsteady behavior of the discharge potential, we are taken the electrode current as the known (and constant) parameter, and the electrode potential as the unknown.

Figure 7 presents the dimensionless sheath magnitudes for the active electrode. Both the non-dimensional current to the electrode sheath and the relationship between the emitted electron flux and net electron flux coming from the sheath are shown, for sonic and supersonic ion fluxes (see 9). The higher the potential fall in the wall, the higher is the electric current. Notice that moderate sheath potential falls enough to emit a significant electric current.
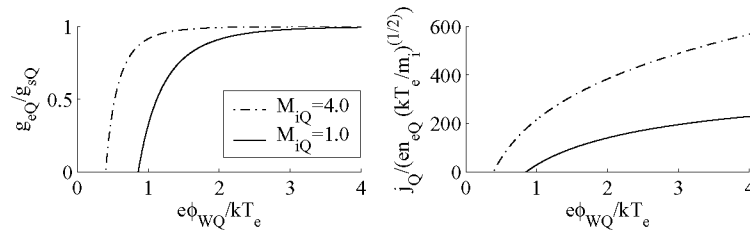
Figure 7. Net electron wall flux to electron emitted flux ratio (left) and non-dimensional wall current(right) as functions of the non-dimensional sheath potential fall for a high-emission electrode.

B.   Electron subcode with variable discharge current

The electron subcode of HPHall-2 was designed for ceramic walls only and thus considered that the discharge current was constant along the channel. This simplified enormously the electron continuity equation. The present code eliminates that constraint by accepting net exchanges of electric current at the lateral walls. The continuity equation, averaged over a magnetic streamsurface, becomes

$$\frac{\partial I_d}{\partial \lambda} = -\frac{2\pi j_{s_1}}{(B\cos\alpha)|_1} - \frac{2\pi j_{s_2}}{(B\cos\alpha)|_2} \tag{2}$$

where λ is the magnetic stream function, $I_d(\lambda)$ is the variable discharge current, $j_{s_1}(\lambda)$ and $j_{s_2}(\lambda)$ are the electric density currents to the inner(1) and outer(2) walls, and $\alpha(\lambda)$ is the angle between the wall normal and the magnetic field. Equation(2) is coupled with quasi-1D expressions for the electron energy equation and the Ohm´s generalized law. These equations depend only on one spatial variable, λ, thanks to the assumptions of constant electron temperature and Boltzmann equilibrium along magnetic field lines. The advantages of a differential formulation, compared to the integral one, is that it gives more flexibility on the choice of the most convenient numerical integration algorithm. Also, in the new code, we are trying to make the magnetic mesh [Fig.1(c)] fully independent from the PIC-mesh [Fig. 1(a)]. In this manner, refinement

can be achieved in the electron subcode without increasing the number of cells of the PIC-mesh. Besides, non-uniform electron meshes can be used to better model electron physics. Finally, the new formulation has allowed to account for the work of the electric field parallel to magnetic field lines, neglected in HPHall-2.

C.   Results

Figure 8 and table 3 show the profiles of the main plasma variables and performance parameters when an intermediate electrode 2mm wide, located at z=21mm on the outer wall, and emits different electric currents. Rest of parameters remain nominal, even the magnetic field strength and profile. Both propellant and voltage utilization tend to increase when augmenting the electrode current. However, since the magnetic field has not been optimized (as Ahedo and Parra[6] did) the current utilization and thus the anode efficiency decrease.
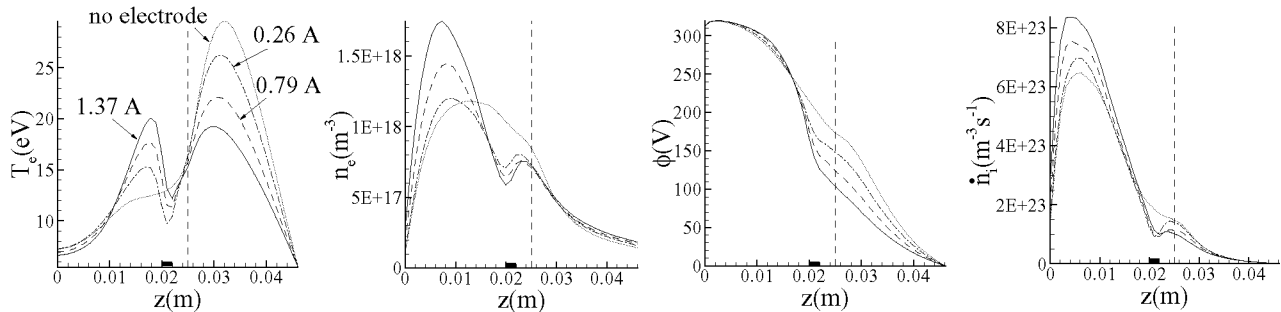
Figure 8. Electron temperature, T_e, electron density, n_e, electric potential, ϕ, and total ionization rate, $\dot{n}_i$, profiles for different currents through the electrode. The electrode is 2mm wide and is located on the outer wall at axial position z=21mm. The vertical dashed line represents the thruster exit.

$I_{electrode}(A)$	η_a	$I_{sp}(s)$	η_{cur}	η_u	$\eta_{vol,i+}$	$\eta_{p,i+}$
no electrode	0.40	1360	0.80	0.77	0.79	0.75
0.26	0.42	1443	0.78	0.81	0.80	0.78
0.79	0.37	1408	0.70	0.78	0.81	0.78
1.37	0.33	1380	0.62	0.75	0.81	0.79

Table 3.   Performance parameters for different currents through the electrode corresponding to figure 8.

Figure 9 displays the different profiles for the main variables when modifying the electrode location and maintaining almost constant the electrode current. Corresponding performance variables are shown in table 4. It is clear that the electrode location affects the thruster response. In fact, in the new electrode location (z=16mm) the anode efficiency is higher than in the previous case. This influence agrees well with the conclusions of Ahedo and Parra.[6] We remind again that the current utilization is very low due to the non-optimal magnetic field.

$z_{electrode}(mm)$	$I_{electrode}(A)$	η_a	$I_{sp}(s)$	η_{cur}	η_u	$\eta_{vol,i+}$	$\eta_{p,i+}$
-	no electrode	0.40	1360	0.80	0.77	0.79	0.75
21	1.37	0.33	1380	0.62	0.75	0.81	0.79
16	1.46	0.37	1550	0.61	0.82	0.87	0.81

Table 4.   Performance parameters for different electrode locations corresponding to figure 9.
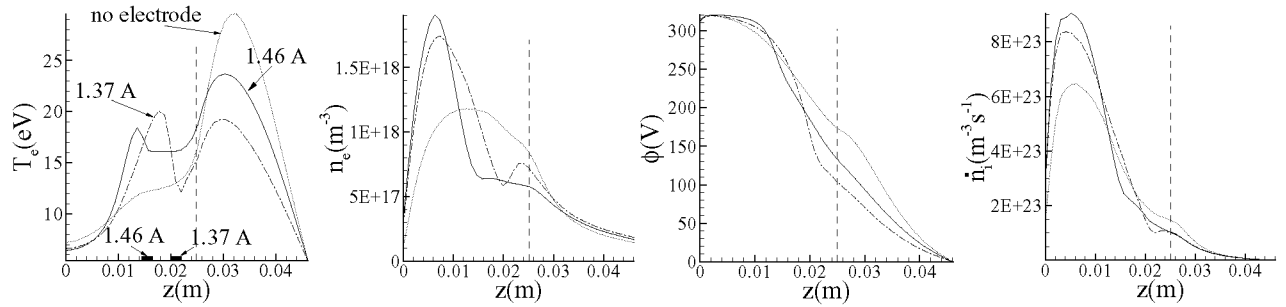
Figure 9. Electron temperature, T_e, electron density, n_e, electric potential, ϕ, and total ionization rate, $\dot{n}_i$, profiles for different location of the electrode and similar currents. Electrode is located on the outer wall at axial positions z=0.021m and z=0.016m respectively. In both cases the electrode is 2mm wide. The vertical dashed line represents the thruster exit.

V. Wall erosion

The most important process limiting the lifetime of Hall thrusters is the erosion of the ceramic walls. The main erosion mechanism is produced by ion impact. The local erosion rate can be modelled by[17]

$$\frac{dh}{dt} = c \cdot X(\dot{\epsilon}) \cdot Y(\theta) \tag{3}$$

where h is the erosion depth, $X(\dot{\epsilon})$ and $Y(\theta)$ are functions of the ion energy flux and the impact angle with the wall, respectively, and c is a constant that depends on the material composition.

There are few published results on material sputtering properties. In the simulations presented below we have used the experimental results of Kim et al.,[18] which show a linear dependence with the energy flux (i.e. $X(\dot{\epsilon}) = \dot{\epsilon}$) and a relative maximum of $Y(\theta)$ for $\theta \sim 50 - 60^{o}$, with $Y(55^{o})/Y(0^{o}) \sim 300\%$. The adapted form of the erosion law to the PIC methodology is

$$\Delta h(t_{op}) = \frac{t_{op} \, c}{t_{sim} \Delta S} \sum_{\forall \Delta t} \sum_{p} \frac{m_p v_p^2}{2} Y(\theta_p) \tag{4}$$

where Δh is computed for each wall panel, ΔS is the panel area, summation on p applies to the particles (ions) p crossing the panel within each time interval; summation on Δt apply to the time steps of the simulation; $t_{sim} = \sum_{\forall \Delta t} \Delta t$ is the operational time of one simulation, and t_{op} is the real time of operation of the thruster. Figure 10(a) shows five stages of erosion at the inner and outer walls of the thruster and the total time of operation of the thruster to reach each of them. Each stage corresponds approximately to 1mm erosion of each wall at the exit section of the chamber. The value of t_{op} in the figure is based on a sputtering constant of the material of $c = 10^{-4} (\mu\text{m/h})/(\text{W/m}^2)$; for other values of c, just take $t_{op} \propto c^{-1}$. After each erosion stage, the simulation code modifies accordingly the channel geometry and runs a new simulation of the discharge to update the thruster performances for the next erosion stage. Figures 10(b)-(c) show the changes in efficiency and total ion energy flux to the walls $P_{i,wall}$ as the erosion progresses. The decrease of $P_{i,wall}$ as the annular channel becomes weakly divergent explains the slowing down of erosion; this trend is well documented experimentally. Since the ion flux to the walls is more or less proportional to $P_{i,wall}$, it decreases too as t_{op} increases. As a consequence, electron energy losses decrease, thus explaining the increase in efficiency.

Figure 11 displays 2D profiles of the plasma behavior in the initial and final stages of the preceding figure. The plasma density decreases mildly because of the larger discharge channel, mainly near the exit. This moves the ionization region closer to the anode. Related to this are a decrease of the electric field in the acceleration region and a gentler temperature profile.

The simulation based on the sputtering law 3, with a linear dependence on the ion energy, implies that the channel is eroded up to the anode. However, some experimental results would indicate that only the
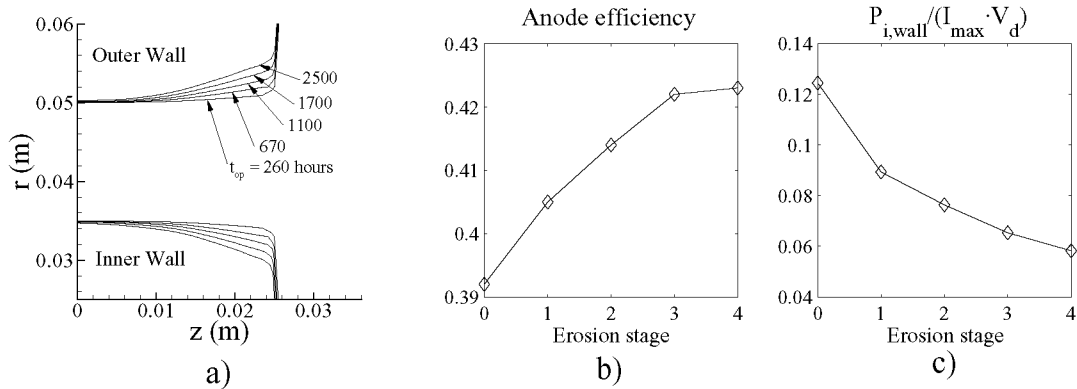
Figure 10. (a) **Wall profiles at different erosion stages;** t_{op} **is the total operation time.** (b)**Efficiency and (c) total ion energy deposition at the walls after each erosion stage;** $I_{max} = e\dot{m}_a/m_i$.

downstream region of the channel is effectively eroded.[19,20] We have two possible explanations in mind. First, the experimental plasma discharge has the ionization region closer to the exit. Second, the dependence of erosion on the ion energy is not linear for low energies; instead a certain threshold would exist.

VI. Conclusions

This paper has summarized the advances made on the 2D modelization of Hall thruster physics and the expected capabilities of a new 2D hybrid simulation code, specially those referred to the simulation of high-specific-impulse operation and two-stage type designs. Reference[9] complements this paper. The results we present can only be seen as preliminary since the code is being constructed still and results have not been checked carefully.

Acknowledgments

References

[1]R.S.Jankovsky, Jacobson, D. T., Sarmiento, C. J., Piñero, L. R., Manzella, D. H., Hofer, R. R., and Peterson, P. Y., "NASA's Hall thruster program 2002," *38th Joint Propulsion Conference, Indianapolis, IN*, AIAA 2002-3675, American Institute of Aeronautics and Astronautics,Washington, DC, 2002.

[2]Hofer, R. R. and Gallimore, A. D., "Efficiency Analysis of a High-Specific Impulse Hall Thruster," *40th Joint Propulsion Conference, Fort Lauderdale, FL*, AIAA-2004-3602, American Institute of Aeronautics and Astronautics,Washington, DC, 2004.

[3]Yamagiwa, Y. and Kuriki, K., "Performance of double-stage-discharge Hall ion thruster," *J. Propulsion and Power*, Vol. 7, No. 1, 1991, pp. 65–70.

[4]Pote, B. and Tedrake, R., "Performance of a high specific impulse Hall thruster," *27th International Electric Propulsion Conference, Pasadena, CA, USA*, IEPC-01-035, Electric Rocket Propulsion Society, Cleveland, OH, 2001.

[5]Hofer, R., Peterson, P., Gallimore, A., and Jankovsky, R., "A high specific impulse two-stage Hall thruster with plasma lens focusing," *7th International Electric Propulsion Conference, Pasadena, CA, USA*, IEPC-01-036, Electric Rocket Propulsion Society, Cleveland, OH, 2001.

[6]Ahedo, E. and Parra, F., "A model of the two-stage Hall thruster discharge," *Journal of Applied Physics*, Vol. 98, 2005, pp. 023303.

[7]Parra, F., Ahedo, E., Martínez-Sánchez, M., and Fife, M., "A two-dimensional hybrid model of the Hall thruster discharge," (to be submitted).

[8]Fife, J. M., *Hybrid-PIC Modeling and Electrostatic Probe Survey of Hall Thrusters*, Ph.D. thesis, Massachusetts Institute of Technology, 1998.
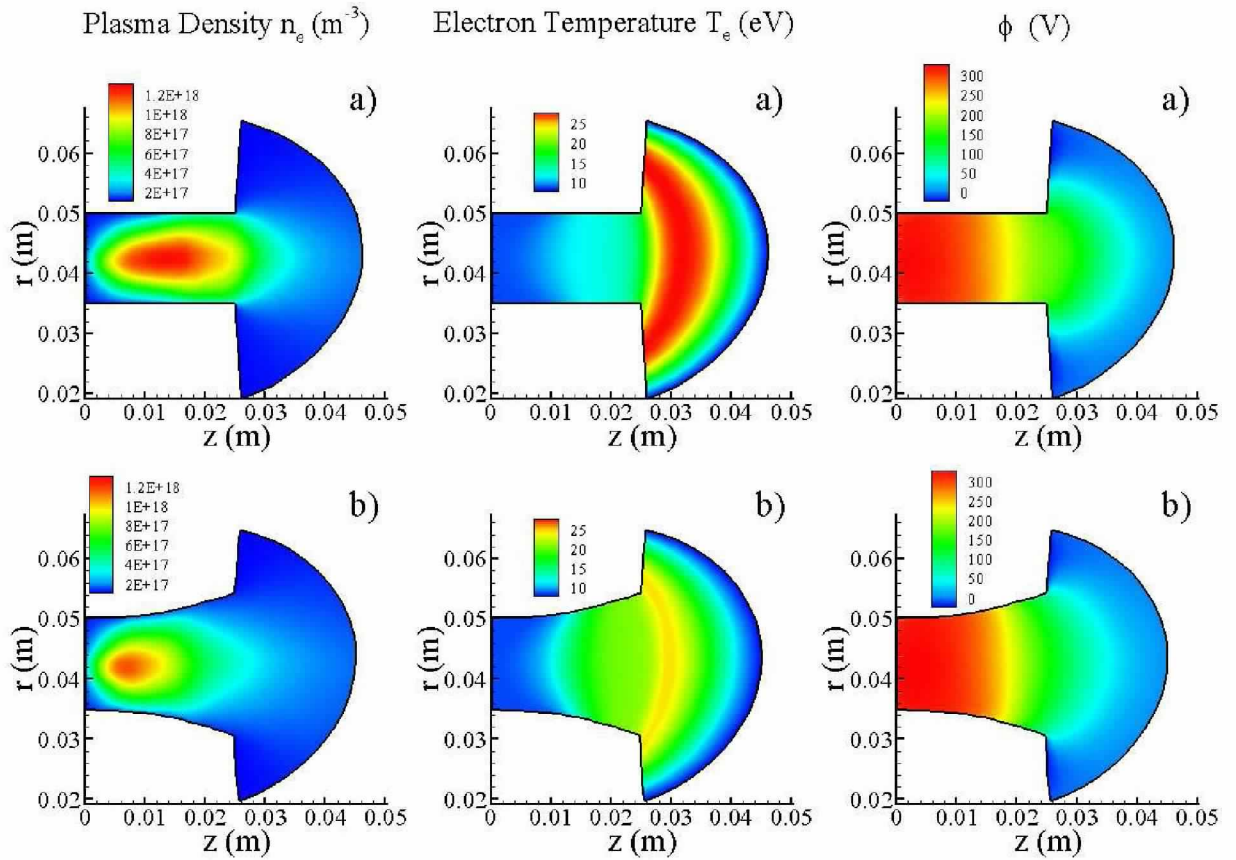
Figure 11. Electron density, $n_e(\mathrm{m}^{-3})$, electron temperature, T_e and electric potential, ϕ, 2D plots at the initial(a) and final(b) stages of erosion.

[9]Escobar, D., Ahedo, E., and Parra, F. I., "On conditions at the sheath boundaries in a quasineutral code for Hall thrusters," *Proc. 29th International Electric Propulsion Conference, Princeton, USA*, IEPC-2005-041, Electric Rocket Propulsion Society, Cleveland, OH, 2005.

[10]Ahedo, E., de Pablo, V., and Martínez-Sánchez, M., "Effects of partial thermalization and secondary emission on the electron distribution function of Hall thrusters," *Proc. 29th International Electric Propulsion Conference, Princeton, USA*, IEPC-2005-118, Electric Rocket Propulsion Society, Cleveland, OH, 2005.

[11]Gallardo, J. and Ahedo, E., "On the anomalous diffusion mechanism in Hall thrusters," *Proc. 29th International Electric Propulsion Conference, Princeton, USA*, IEPC-2005-117, Electric Rocket Propulsion Society, Cleveland, OH, 2005.

[12]Meezan, N. and Capelli, M., "Kinetic study of wall collisions in a coaxial Hall discharge ," *Physical Review E*, Vol. 66, 2002, pp. 036401.

[13]Batishev, O. and Martínez-Sánchez, M., "Charge particle transport in the Hall effect thruster," *Proc. 28th International Electric Propulsion Conference, Toulouse, France*, Electric Rocket Propulsion Society, Cleveland, OH, 2003.

[14]Barral, S., Makowski, K., Peradzynski, Z., Gascon, N., and Dudeck, M., "Wall material effects in stationary plasma thrusters. II. Near-wall and in-wall conductivity ," *Phys. Plasmas*, Vol. 10, No. 10, 2003, pp. 4137 – 4152.

[15]Ahedo, E. and Parra, F., "Partial trapping of secondary electron emission in a Hall thruster plasma," *Physics of Plasmas*, Vol. 12, No. 7, 2005, pp. 073503.

[16]Ahedo, E., "Presheath/sheath model of a plasma with secondary emission from two parallel walls," *Physics of Plasmas*, Vol. 9, No. 10, 2002, pp. 4340–4347.

[17]Kim, V., "Main physical features and processes determining the performance of stationary plasma thrusters," *J. Propulsion Power*, Vol. 14, No. 5, 1998, pp. 736–743.

[18]Kim, V., Kozlov, V., Semenov, A., and Shkarban, I., "Investigation of the Boron Nitride based ceramics sputtering yield under its bombardment by Xe and Kr ions," *27th International Electric Propulsion Conference, Pasadena, CA, USA*, IEPC 01-073, Electric Rocket Propulsion Society, Cleveland, OH, 2001.

[19]Kim, V., Kozlov, V., Skrylnikov, V., Hilleret, N., Henrist, B., Locke, S., and Fife, M., "Investigation of operation and characteristics of small SPT with discharge chamber walls made of different ceramics," *39th Joint Propulsion Conference, Huntsville, AL*, AIAA 2003-5002, American Institute of Aeronautics and Astronautics,Washington, DC, 2003.

[20]Peterson, P. and Manzella, D., "Investigation of the erosion characteristics of a laboratory Hall thruster," *39th Joint Propulsion Conference, Huntsville, AL,* AIAA 2003-5005, American Institute of Aeronautics and Astronautics,Washington, DC, 2003.

Appendix: Efficiency definitions

When we analyze the efficiency of the plasma discharge on the performance of a Hall thruster, the natural parameter is the so-called anode efficiency

$$\eta_a = \frac{F^2}{2\dot{m}_a P_d} \tag{5}$$

where F is the thrust, $\dot{m}_a$ is the mass flow through the anode and P_d is the electrical power to sustain electrode and cathode currents; for a simple, single-stage thruster, $P_d = I_d V_d$. The anode efficiency can be split up into several partial efficiencies accounting each one for a different process inside the thruster. Thus, we write

$$\eta_a = K \, \eta_u \, \eta_{cur} \, \eta_q \, \eta_{vol,i+} \, \eta_{p,i+} \tag{6}$$

where

$$\eta_u = \frac{\dot{m}_{i,c}}{\dot{m}_a} \tag{7}$$

is the mass or propellant utilization (subscripts a and c refer to the anode and the streamsurface containing the virtual cathode, respectively);

$$\eta_{cur} = \frac{I_{di,c} V_d}{P_d} \tag{8}$$

is the current utilization (it represents the additional necessary electron current to maintain the thruster operation and can also be considered a way to characterize the ionization process);

$$\eta_{vol,i+} = \frac{P_{jet,i+}}{I_{di+,c} V_d} \tag{9}$$

is the voltage utilization based on singly-charged ion acceleration ($P_{jet,i+}$ is the singly-charged ion jet power at the domain exit);

$$\eta_{p,i+} = \frac{F_{i+}^2 / 2\dot{m}_{i+,c}}{P_{jet,i+}} \tag{10}$$

is a plume-divergence efficiency, based on singly-charged ion magnitudes (F_{i+} is the thrust due exclusively to singly-charged ions);

$$\eta_q = \frac{(I_{di+,c} + I_{di++,c}/\sqrt{2})^2}{(I_{di+,c} + I_{di++,c})(I_{di+,c} + I_{di++,c}/2)} \tag{11}$$

is the charge utilization ($I_{di+,c}$ and $I_{di++,c}$ are singly- and doubly-charged ion currents), which measures the influence of doubly-charged ions on the thrust ; and K accounts for minor contributions to η_a like the part of the thrust due to neutrals and electrons.